Mutations of PI3K-AKT-mTOR Pathway as Predictors for Immune Cell Infiltration and Immunotherapy Efficacy in dMMR/MSI-H Gastric Adenocarcinoma

zhenghang wang
Peking University Cancer Hospital: Beijing Cancer Hospital
Xinyu Wang
Peking University Cancer Hospital: Beijing Cancer Hospital
Yu Xu
3D Medicines Lnc
Jian Li
Peking University Cancer Hospital: Beijing Cancer Hospital
Xiaotian Zhang
Peking University Cancer Hospital: Beijing Cancer Hospital
Zhi Peng
Peking University Cancer Hospital: Beijing Cancer Hospital
Yajie Hu
Peking University Cancer Hospital: Beijing Cancer Hospital
Xinya Zhao
Peking University Cancer Hospital: Beijing Cancer Hospital
Kun Dong
Peking University Cancer Hospital: Beijing Cancer Hospital
Bei Zhang
3D Medicines Lnc
Chan Gao
3D Medicines Lnc
Xiaochen Zhao
3D Medicines Lnc
Hui Chen
3D Medicines Lnc
Jinping Cai
3D Medicines Lnc
Yuezong Bai
Peking University Cancer Hospital: Beijing Cancer Hospital

Yu Sun
Peking University Cancer Hospital: Beijing Cancer Hospital
Lin Shen (shenlin@bjmu.edu.cn)
Peking University Cancer Hospital: Beijing Cancer Hospital https://orcid.org/0000-0002-8798-4756

Research

Keywords: dMMR/MSI-H gastric adenocarcinoma, PI3K-AKT-mTOR pathway, tumor-infiltrating immune cell, immune checkpoint inhibitor

Posted Date: October 5th, 2021

DOI: https://doi.org/10.21203/rs.3.rs-929879/v1

Version of Record: A version of this preprint was published at BMC Medicine on April 21st, 2022. See the published version at https://doi.org/10.1186/s12916-022-02327-y.

Abstract

Background: A significant subset of mismatch repair-deficient (dMMR)/microsatellite instability-high (MSI-H) gastric adenocarcinomas (GAC) are resistant to immune checkpoint inhibitors (ICIs), yet the underlying mechanism remains largely unknown. We sought to investigate the genomic correlates of the density of tumor-infiltrating immune cells (DTICs) and primary resistance to ICI treatment.

Methods: Four independent cohorts of MSI-H GAC were included: (i) the surgery cohort (n=175) with genomic and DTIC data, (ii) the 3DMed cohort (n=32) with genomic and PD-L1 data, (iii) the Cancer Genome Atlas (TCGA) cohort (n=73) with genomic, transcriptomic, and survival data and (iv) the ICI treatment cohort (n=36) with pre-treatment genomic profile and ICI efficacy data.

Results: In the dMMR/MSI-H GAC, the **n**umber of **m**utated genes in the **P**I3K-AKT-mTOR pathway (NMP) was positively correlated with tumor mutational burden (P<0.001) and sensitivity to PI3K-AKT-mTOR inhibitors, and negatively correlated with $CD3^+$ (P<0.001), $CD4^+$ (P=0.065), $CD8^+$ (P=0.004), and $FOXP3^+$ cells (P=0.033) in the central-tumor rather than invasive-margin area, and the transcription of immune-related genes. Compared to the NMP-low (NMP=0/1) patients, the NMP-high (NMP≥2) patients exhibited a poorer objective response rate (29.4% vs. 85.7%, P<0.001), progression-free survival (HR=3.40, P=0.019), and overall survival (HR=3.59, P=0.048) upon ICI treatment.

Conclusion: Higher NMP was identified as a potential predictor of lower DTICs and primary resistance to ICIs in the dMMR/MSI-H GAC. Our results highlight the possibility of using mutational data to estimate DTICs and administering the PI3K-AKT-mTOR inhibitor as an immunotherapeutic adjuvant in NMP-high subpopulation to overcome the resistance to ICIs.

Background

A mismatch repair-deficient/microsatellite instability-high (dMMR/MSI-H) phenotype often leads to a buildup of base-pair mismatches and slippage events over time [1–3], eventually causing high rates of insertions and deletions (indels) of nucleotides in microsatellites sequences [4]. The dMMR/MSI-H tumors are characterized by a high load of frameshift mutations and neoantigens, facilitating immune recognition and immune cell infiltration [5–7]. These infiltrating immune cells are commonly exhausted with upregulation of checkpoint proteins, including programmed death 1 (PD-1) and programmed death-ligand 1 (PD-L1), which serve as the targets of anti-PD-1/PD-L1 immunotherapy [8–10].

In theory, dMMR/MSI-H solid tumors should acquire favorable benefits from immune checkpoint inhibitor (ICI) treatment, yet nearly 40% of them had progressive disease as best response [11, 12], suggesting the heterogeneity within this hypermutated subtype. Previous studies in MSI-H gastric adenocarcinoma (GAC) and colorectal cancer (CRC) suggested the association between mRNA-based clusters and survival of ICI therapy [13, 14]. However, little is known about the heterogeneity of immune-related features in MSI-H tumors, including the density of tumor-infiltrating immune cells (DTICs). A better understanding of the

heterogeneity within these hypermutated tumor subsets and the unrecognized mechanism of resistance to ICIs is crucial for patient selection.

GAC is a major cause of cancer deaths worldwide [15]. It is one of the solid tumors with high microsatellite instability [11, 16–18] and is characterized by high abundant leukocyte infiltration, high proportion of activated immunophenotype, and strong correlation between clonal heterogeneity and immunophenotype [19]. Therefore, we were interested to see whether GAC patients with dMMR/MSI-H could be further dissected according to their immune-related features by depicting the mutational landscape of dMMR/MSI-H GAC, and further investigate the genomic correlates of immune cell infiltration and clinical benefits from ICI treatment.

Methods

Patients

In the surgery cohort (**Supplementary Figure S1**), 175 patients with resected primary gastric or gastro-esophageal junction (G/GEJ) cancer treated at Peking University Cancer Hospital and Institute from December 14, 2015, to November 13, 2019, were included. All tumors were evaluated by immunohistochemistry (IHC) to assess the expression of MMR proteins and were assigned a pathological tumor, node, and metastases (TNM) stage. This cohort was initially employed for a double-blinded technical validation of a 9-loci polymerase chain reaction (PCR) testing to identify MSI-H. Herein we retrieved the patients' MSI status as determined by tissue-PCR of the pentaplex (BAT26, NR24, NR21, MONO27, and BAT25) and by next-generation sequencing (NGS) using a 733-gene panel incorporating 100 MSI loci (3D Medicines, Inc., Shanghai, China).

The 3DMed cohort consisted of 32 cases, selected from the 51718 cases of the 3D Medicines database tested between January 6, 2017, and April 14, 2020. Cases were included only if they had PD-L1 expression data as evaluated by PD-L1 IHC 22C3 pharmDx (Dako, Inc.), and genomic profiling data by NGS using a 381-gene panel (**Supplementary Figure S1B**).

The Cancer Genome Atlas (TCGA) cohort (n = 73) was obtained from the PanCancer stomach adenocarcinoma (STAD) dataset (**Supplementary Figure S1C**), where patients were included if they had available mutational and transcriptional data, and an MSI-H phenotype diagnosed by the TCGA subtyping system [20]. Missense mutations in this cohort were evaluated by both Polyphen-2 and Sorting Intolerant From Tolerant (SIFT) [21, 22], to filter out potential benign alterations. Gene set enrichment analysis (GSEA) was performed to investigate the transcriptional difference.

The ICI treatment cohort (n = 36) was retrieved from the medical records of the Department of Gastrointestinal Oncology, Peking University Cancer Hospital and Institute, where patients with dMMR/MSI-H GAC received at least 1 cycle of any ICI treatment regardless of the agent's target (PD-1, PD-L1, or CTLA-4) from September 1, 2017, to January 31, 2020, had their last follow-up before June 1, 2021, and had NGS-based mutational data of pre-treatment tissue or plasma (**Supplementary Figure S1D**).

Moreover, ten patients had available data of pre-treatment peripheral blood lymphocyte subset counts via flow cytometry.

IHC, PCR, NGS, GSEA, analysis of drug sensitivity, flow cytometry, multiplex immunofluorescence, and assessment of tumor response are described in **Supplemental Methods S1-7** and **Supplemental Table S1-7**.

Human samples and clinical data were collected and used in accordance with the principles of the Declaration of Helsinki and approved by the Ethics committee of Peking University Cancer Hospital. All participants provided written informed consents. This report followed the Strengthening the Reporting of Observational Studies in Epidemiology (STROBE) reporting guideline.

Statistical analysis

The significance with categorical variables was evaluated by Fisher's exact test. The significance with disease-free survival (DFS), progression-free survival (PFS), and overall survival (OS) was assessed by the Log-rank method. Univariable and multivariable Cox regression was implemented to calculate the hazard ratio (HR) of survival data. The significance with continuous variables was assessed by non-parametric tests (e.g., rank-sum tests, Spearman correlation test) or corrected parametric tests for variance correction (e.g., unpaired t-test with Welch's correction). Receiver operating characteristic (ROC) curve and area under the curve (AUC) were used for seeking the best cut-off of the number of mutated genes in the PI3K-AKT-mTOR pathway (NMP) for predicting immunotherapeutic efficacy. All statistical analyses mentioned above were performed using IBM SPSS Statistics 22, and the graphs were drawn by GraphPad Prism 8 and RStudio (version 1.2.5042). We set the nominal level of significance as 5%, and all 95% CIs were 2-sided.

Results

Clinicopathological and genomic features of dMMR/MSI-H GAC.

The clinicopathological and genomic features of 175 resected samples from patients with primary G/GEJ adenocarcinoma are described in **Supplementary Table S5** and **Figure 1A**. IHC, PCR (5 loci), and NGS (100 loci) testing identified 115 concordant-dMMR/MSI-H samples, 46 concordant MMR-proficent (pMMR)/microsatellite stable (MSS) samples, and 14 discordant samples. The distribution of MSI score (by NGS testing), PCR score, and IHC result are displayed in **Supplemental Figure S2** and **Supplemental Table S6**. In the 161 samples with concordant results of IHC and PCR testing, NGS was able to correctly detect MSI status with 100% sensitivity and 100% specificity. Furthermore, among the 14 samples where IHC result showed incomplete loss of MMR protein expression (e.g., loss of MSH6 expression in 50% of tumor cells and intact expression of MLH1/PMS2/MSH2) or was inconsistent with PCR results (e.g., IHC-dMMR but PCR-MSS), NGS identified 7 NGS-MSI-H cases with the highest variability of the tested microsatellites and the highest frameshift burden in the tested coding sequence (**Supplemental Table**

S7). Taken together, NGS performed better in identifying MSI-H cases compared to IHC and PCR, especially when geographical heterogeneity of MMR protein expression is observed, or IHC and PCR results are inconsistent.

Among the concordant samples, dMMR/MSI-H status was associated with an early tumor stage (P=0.050), intestinal type of Lauren classification (P=0.058), lower HER2 expression (P=0.034), and EBV negativity (P=0.008, **Supplementary Table S5**). As for genetic aberration, mutations of *TP53* (P=0.021) and *CCNE1* (P=0.003) were enriched in pMMR/MSS samples, while the mutations in *ARID1A*, *ACVR2A*, *KMT2C*, *TGFBR2*, *KMT2D,* and *RNF43* genes were dominant in dMMR/MSI-H samples (P<0.001) with mutational frequencies over 70% (**Figure 1B**). Significantly higher tumor mutational burden (TMB) and the numbers of frameshift mutation, missense mutation, non-frameshift insertion and deletion (indel), stopgain mutation, and splice site mutation were observed in concordant dMMR/MSI-H cases. On the contrary, copy number variation (CNV) and fusion were enriched in concordant pMMR/MSS cases (**Supplemental Table S5** and **Figure 1C**).

Most dMMR/MSI-H samples carried mutations in the DNA damage response (99%), chromatin remodeling (99%), WNT (99%), TGFβ (98%), PI3K-AKT-mTOR (91%), Hippo (90%), and NOTCH (90%) pathways, while relatively lower mutational rates were discovered in the RTKs (73%), Hedgehog (68%), cell cycle (63%), Ras-Raf-MEK-ERK/JNK (62%), p53 (56%), and telomere maintenance (19%) pathways (**Figure 1D**). In the dMMR/MSI-H tumors with such high mutational burden and intratumoral heterogeneity, a singular mutation (e.g., *PTEN* mutation) can hardly reflect the functional alteration of the whole pathway (the PI3K-AKT-mTOR pathway) and the overall characteristics of the tumor. Therefore, we sought to define the number of mutated genes in the pre-specified pathway as a parameter representing the pathway's potential changes and to explore its correlation with the density of DTICs and response to ICI treatment in the dMMR/MSI-H GAC.

Correlates of DTIC in dMMR/MSI-H GAC

Of the 115 concordant-dMMR/MSI-H cases, the evaluation of DTICs was missing in twelve cases (**Supplementary Table S8**), and another fourteen cases were excluded for prior neoadjuvant chemotherapy which could affect DTICs (**Supplementary Table S9**) [23-25]. Therefore, 89 samples were included for the following analysis of genomic correlates of DTICs.

A comprehensive correlation matrix was created to seek the correlates of DTICs, including $CD3^+$, $CD4^+$, $CD8^+$, $CD68^+$, and $FOXP3^+$ cells in central-tumor and invasive-margin areas (**Figure 2**). Among the clinicopathological and genomic characteristics, the **n**umber of **m**utated members in the **P**I3K-AKT-mTOR pathway (NMP) exhibited the strongest negative correlation with DTICs, including $CD3^+$ (P<0.001), $CD4^+$ (P=0.065), $CD8^+$ (P=0.004), and $FOXP3^+$ (P=0.033) cells in central tumor area (marked by a red arrow, **Figure 2**). The correlations of NMP with central-tumor DTICs were markedly stronger than its correlations with invasive-margin DTICs, suggesting the potential difference of PI3K-AKT-mTOR function in central

tumor and invasive margin. Sensitivity analysis further indicated the robustness of the above-mentioned results (**Supplementary Table S10**). The mutations of the members in the PI3K-AKT-mTOR pathway are illustrated in **Supplementary Figure S3**. The scatter diagrams of the above-mentioned results and representative images of immunohistochemical staining of tumor-infiltrating immune cells are displayed in **Figure 3**.

Of note, TMB was strongly correlated with nearly all the numbers of mutated members in the pre-specified pathways (marked by a purple arrow, **Figure 2**) including the PI3K-AKT-mTOR pathway, rather than DITCs (marked by a blue arrow, **Figure 2**), consistent with previous results in MSI-H CRC [14, 26].

Given the correlations of NMP with DTICs, we next sought to investigate the associations of NMP with other potential predictors of immunotherapy, including TMB, PD-L1 expression, and immune-related mRNA signatures.

Biological characteristics of the DTIC-enriched subtype with lower NMP

Since higher TMB and PD-L1 levels were commonly associated with more clinical benefit from ICI treatment in microsatellite stable (MSS) G/GEJ cancer [27-34] and two recent retrospective studies with small sample size suggested the association between TMB and immunotherapy efficacy in MSI-H GAC [35, 36], we set out to evaluate TMB and PD-L1 expression in the DTIC-enriched subtype of MSI-H GAC with lower NMP.

We retrieved the data of 32 MSI-H GACs (primary lesion) with assessments of mutations and PD-L1 from the 3DMed database. Among these, lower NMP was correlated with lower TMB (P<0.001, **Figure 4A**), but not the PD-L1 expression in tumoral and immune cells (tumor proportion score [TPS]: P=0.961; immune proportion score [IPS]: 0.484; combined positive score [CPS]: P=0.699; **Figure 4B**). Detailed characteristics and data are shown in **Supplementary Table S11**. The representative images of PD-L1 staining are shown in **Figure 4C**, and the images of corresponding hematoxylin-eosin (HE) staining and positive/negative controls are enclosed in **Supplementary Figure S4**.

Immune-related gene signatures were further explored in the TCGA cohort by GSEA (characteristics are shown in **Supplementary Table S12**). Multiple significant enrichments of immune-related signatures were revealed in the PI3K-AKT-mTOR^{WT} group (**Figure 4D**), including MHC-II-mediated antigen presentation (P=0.001), cross presentation (P=0.001), B cell receptor downstream signaling (P=0.017), T cell receptor downstream signaling (P<0.001), interferon signaling (P=0.045), and PD-1 signaling (P=0.006), while the activity of TGFβ signaling was decreased in the PI3K-AKT-mTOR^{WT} group (P<0.001). Of note, despite the enrichment of PD-1 signaling in PI3K-AKT-mTOR^{WT} group, the mRNA expression of *CD274* (PD-L1) was not higher in PI3K-AKT-mTOR^{WT} group than in PI3K-AKT-mTOR^{mut} group, suggesting that PD-L1 expression is irrelevant to PI3K-AKT-mTOR mutations (P=0.341), consistent with the results in **Figure 4B**.

Similar enrichments in the PI3K-AKT-mTOR^{WT} group were observed in interleukin (IL) pathways, including IL-1 (P=0.031), IL-12 (P=0.014), and IL-12 family (P=0.059, **Figure 4E**).

In addition to the immune-related gene signatures, we further assessed the signatures of NOTCH signaling. We previously reported that the downregulation of NOTCH pathway was associated with higher level of immune gene transcription and better immunotherapeutic efficacy in non-small cell lung cancer (NSCLC) [37]. Here, in the MSI-H GACs, the DTIC-enriched PI3K-AKT-mTOR^{WT} group displayed trends towards downregulation of NOTCH-related signatures, especially the ones concerning transcriptional impact (**Figure 4F**).

PI3K-AKT-mTOR inhibitor efficacy of MSI-H GAC cell lines with different NMPs

Furthermore, we aimed to discover the association between PI3K-AKT-mTOR mutation and drug sensitivity. Among the five MSI-H GAC cell lines (NUGC-3, TGBC11TKB, SNU-1, IM95, and 23132/87), NUGC-3 and TGBC11TKB had two mutations of the members of the PI3K-AKT-mTOR pathway, and SNU-1, IM95, and 23132/87 had no less than four member mutations (**Figure 4G**). The PI3K-AKT-mTOR inhibitors (targeting AKT/mTORC/PDK1/PI3K/S6K1) exhibited lower IC_{50} in the SNU-1, IM95, and 23132/87 cell lines (P<0.001) than in NUGC-3 and TGBC11TKB cell lines, and the inhibitors targeting VEGFR (P=0.142) or EGFR (P=0.540) and chemotherapeutic drugs (P=0.378) showed no significant difference of sensitivity (**Figure 4G**). Taken together, these results indicate that the MSI-H STADs with high NMP might benefit more from PI3K/AKT/mTOR inhibitors, compared to the ones with low NMP.

Immunotherapy efficacy of the DTIC-enriched subtypes with lower NMP

The subtype with lower NMP was characterized by higher DTICs and immune-related gene transcription (potentially associated with better ICI response) [32, 38], and lower TMB (potentially associated with poorer ICI response) [27, 28, 39] in MSI-H GAC. Given these opposite predictive values, we sought to investigate the ICI efficacy of this subtype.

In total, 36 patients with locally advanced or metastatic concordant-dMMR/MSI-H G/GEJ adenocarcinoma were included. The key baseline characteristics, individual response to ICI treatment, and mutational events of the members of the PI3K-AKT-mTOR pathway are illustrated in **Figure 5A** and **Supplementary Table S13**. The best responses are shown in **Figure 5B**. To explore the optimal cut-off of the NMP for predicting immunotherapy efficacy in dMMR/MSI-H G/GEJ adenocarcinoma, a ROC curve was plotted based on the objective response in patients with evaluable target lesion (n=31). The AUC of NMP was significantly higher than 0.5 (AUC=0.792, 95% CI 0.628-0.956, P=0.006, **Figure 5B**), suggesting the feasibility of using NMP to predict response to ICIs. The optimal cut-off was set as 1 when

the largest Youden's index was achieved. In the NMP-high patients (NMP≥2), ORR was 29.4% and 4-month PFS rate was 35.3%, while in the NMP-low patients (NMP=0/1), ORR and 4-month PFS rate were significantly higher as 85.7% (P=0.002) and 93.3% (P=0.001), respectively (**Table 1**).

Consistent with our previous findings, the NMP-high group exhibited higher TMB compared to the NMP-low group (**Figure 5C**), and NMP was not associated with PD-L1 CPS (**Figure 5D**). In addition, the ROC curves based on the objective response demonstrate that TMB (AUC=0.582, 95% CI 0.377-0.787, P=0.44) and PD-L1 CPS (AUC=0.529, 95% CI 0.291-0.767, P=0.82) were not associated with the response to ICI treatment in the dMMR/MSI-H G/GEJ adenocarcinomas (**Supplementary Figure S5**).

The clinical characteristics were comparable between the NMP-high and NMP-low groups (**Supplementary Table S13**). The median time to progression or death was 3.4 months in the NMP-high patients versus not reached in the NMP-low patients (HR=3.40, 95% CI 1.16-10.00, Log-rank P=0.019, **Figure 5E**). Similarly, shorter median OS was observed in the NMP-high patients as 15.0 months, as compared with not reached in the NMP-low patients (HR=3.59, 95% CI 0.94-13.78, Log-rank P=0.048, **Figure 5F**). The maturity of OS was 30.6%, contributing to the slight difference between the results of Cox regression and Log-rank statistics (P=0.063 and 0.048, respectively), and therefore we set PFS as the major outcome in the following analyses.

Despite that higher TMB was observed in the NMP-high group, we found that the predictive effect of NMP on PFS was similar in the TMB-high (≥40 mutations/Mb) and TMB-low (<40 mutations/Mb) subgroups (**Figure 5G**). This cut-off of TMB (40) was selected based on the first study pointing out the predictive effect of TMB in MSI-H gastrointestinal (GI) tumors [39]. Further subgroup analysis suggests the consistent predictive effects of NMP in patients with different characteristics, including treatment lines, ECOG, differentiation grade, PD-L1 CPS, and NGS testing technique (**Figure 5G**). Univariable analyses of PFS and OS did not reveal potential predictive biomarker other than NMP and the multivariable analyses identified NMP as a predictor independent of TMB and PD-L1 for PFS (multivariable HR=5.99, 95% CI 1.21-29.61, P=0.028) and OS (multivariable HR=11.88, 95% CI 1.30-108.4, P=0.028) (**Supplemental Table S14**). Consistent with the results in **Figure 3**, compared to the NMP-high subgroup, higher DTICs, including $CD3^+$ (P=0.022) $CD4^+$ (P=0.013), $CD8^+$ (P=0.10), and $FOXP3^+$ cells (P=0.073) were observed in the NMP-low subgroup by multiplex immunofluorescence, while $CD68^+$ macrophage (P=0.37), M1 macrophage ($CD68^+/CD163^-$, P=0.29), and M2 macrophage ($CD68^+/CD163^+$, P=0.59) were not significantly differed (**Figure 5H-I**).

A previous retrospective study involving 45 dMMR/MSI-H GI tumors (18 gastric tumors) suggests that the mutation of *PTEN*, a key member of the PI3K-AKT-mTOR pathway, was associated with poor response to ICIs [35]. Given this, we first tried to validate this result in our 36 cases and only observed non-significant trends in PFS (P=0.34, **Supplemental Figure S6A**) and OS (P=0.29, **Supplemental Figure S6B**). Moreover, in the 28 $PTEN^{WT}$ cases, NMP-high remained as an indicator of poorer PFS (HR=5.98, 95% CI 1.47-24.22, P=0.005, **Supplemental Figure S6C**) and OS (HR=5.95, 95% CI 1.09-32.47, P=0.022, **Supplemental Figure**

S6D). Taken together, NMP, as a predictor concerning multiple key members of the PI3K-AKT-mTOR pathway, performed more robustly and powerfully than a singular *PTEN* mutation.

In addition, to exclude the possibility that the association between NMP and ICI efficacy was impacted by the pre-treatment immune cell concentration in peripheral blood (reflecting systemic immunity), we detected the correlation between NMP and the pre-treatment status of peripheral blood lymphocyte subsets and observed no significant correlations (**Supplementary Figure S7**). Moreover, PI3K-AKT-$mTOR^{mut}$ was not associated with the DFS (P=0.37) and OS (P=0.37) in the MSI-H GAC cases of the TCGA database (**Supplementary Figure S8**). Collectively, NMP-high was identified as a predictive, rather than prognostic biomarker, associated with inferior clinical benefit from ICI treatment in patients with dMMR/MSI-H G/GEJ adenocarcinoma.

Discussion

This study represents one of the first reports to further dissect dMMR/MSI-H GAC from the aspects including genome, transcriptome, DTIC, and response to ICI treatment. NMP-low was correlated with lower TMB, higher DTICs, greater transcription of immune-related genes, and superior outcome from ICI treatment.

For the surgery cohort which was used to explore associations between specific pathways and DTICs, only samples with IHC-dMMR, PCR-MSI-H and NGS-MSI-H were included. The strict criteria made the following analysis reliable and convincing. In addition, among three methods, NGS demonstrates the perfect accuracy and the potential superiority in identifying MSI-H cases, especially when IHC and PCR results are inconsistent.

DTIC is a crucial predictive biomarker of ICI efficacy [40]. Higher TMB was generally correlated with greater DTICs, due to the immune activation via MHC-mediated neoantigen presentation [41]. However, within the hypermutated MSI-H subtype with numerous neoantigens, the impact of more mutations on greater immune activation might have reached a plateau. In fact, a similar phenomenon has been reported in MSI-H CRC [14, 26]. Consistently, we found no correlation between TMB and DTICs in dMMR/MSI-H GAC. As for the association between TMB and ICI benefit in MSI-H GI cancers, Chida et al. set the cut-off as 10 mutations/Mb to identify TMB-low cases who exhibited poor response to ICI treatment in their MSI-H GI cohort [35]. TCGA network analyzed the pan-GI adenocarcinomas including MSS and MSI-H tumors and defined the MSI subtype by TMB > 10 mutations/Mb, indel burden > 1, and indel/SNV ratio > 1/150 [42]. Based on this, the extremely low TMB (< 10 mutations/Mb) in some MSI-H cases in the study by Chida et al. is more likely to indicate the false positivity of their assessments of MSI-H by PCR and/or dMMR by IHC. In addition, Kwon et al. found that TMB < 26mutations/Mb was associated with poorer PFS on pembrolizumab in a small cohort of MSI-H GAC (n = 15) [36]. However, in our cohort involving 36 G/GEJ adenocarcinomas with concordant MSI-H status by NGS and IHC assessments, the TMB-based AUC for the response to ICI was merely 0.582 (P = 0.44), and no cut-off value can dissect the patients into subgroups with distinct survival outcomes. These findings suggest

that TMB might not be a valid predictive factor for benefit of ICI treatment in MSI-H GAC. Instead, some specific mutated genes and their functional impacts on the DITCs and expression of immune-related genes might be more important in determining the immunotherapy efficacy.

In the tumors with fewer mutations (e.g., MSS and *POLD1*/*POLE*-wildtype GAC), one singular genetic aberration may induce crucial influence. However, in the hypermutated tumors (e.g., MSI-H or *POLD1*/*POLE*-mutant tumors), the effect of a single mutation might be diluted. Therefore, in this study we investigated the association between tumor microenvironments and specific pathways instead of specific gene alterations in the surgery cohort. The degree of pathways' activation was assessed by the number of mutated genes. Among all the pathways we analyzed, the mutated number of the PI3K-AKT-mTOR pathway showed the strongest negative correlation with DTICs. Immune-related signatures were also significantly enriched in the PI3K-AKT-mTOR^{WT} group compared to those in the PI3K-AKT-mTOR^{mut} group. These findings were further validated in MSI-H GAC patients treated with ICIs.

NMP-low tumors (NMP = 0/1) were DTIC-enriched and had better response and longer survival durations on ICI treatment compared to those with high NMP (NMP ≥ 2). Mutations of the members in the PI3K-AKT-mTOR pathway generally activate this signaling [43]. Our results suggest that activated PI3K-AKT-mTOR pathway might be one of the mechanisms underlying immune evasion and primary resistance to immunotherapy in dMMR/MSI-H GAC. Pharmacological inhibition of this pathway not only restored immune-related signal transduction and improved antigen presentation but also increased DTICs, facilitating immune recognition on tumor cells [44–46]. In addition, the impacts of the PI3K-AKT-mTOR pathway on PD-1 signaling might be independent of regulating PD-L1 expression, based on our negative findings and a previous report in melanoma [47].

Preclinical data suggest the upregulation of DTIC via administrating pan-PI3K inhibitor (BKM120), and its synergistic effect with anti-PD-1 in the mouse model bearing breast cancer or muscle-invasive bladder cancer patient-derived xenograft [45, 46]. Our analysis of drug sensitivity in MSI-H GAC cell lines also revealed higher sensitivities to PI3K-AKT-mTOR inhibitors in the cell lines with higher NMP. Currently, multiple trials are ongoing to evaluate the anti-tumor activity of this combination. For example, the NCT03673787 trial (ipatasertib plus atezolizumab) selects patients with pathogenic mutations in *PIK3CA*, *AKT1*, and *AKT2* identified by NGS, or PTEN loss by IHC. Taken together, despite the inferior benefit from ICIs in the NMP-high cases, combination therapy with PI3K-AKT-mTOR inhibitors might be a promising choice to increase DTICs and enhance immunotherapy efficacy in this population.

Although DTICs were associated with ICI efficacy [40], it has not been widely used in clinical practice, due to the lack of standard evaluation method and sufficient tumor samples after the multiple recommended tissue-based assessments, including protein expression of HER2, MMR, and PD-L1 by IHC, and Epstein-Barr virus-encoded small RNA by *in situ* hybridization in gastric cancer. Under these circumstances, NGS testing of circulating tumor DNA (ctDNA), as a technique providing mutational data with high credibility and validity, may be an alternative method to evaluate the DTICs in tumor tissues, by leveraging the correlations between DTICs and genetic aberrations. Meanwhile, given the high level of intratumoral

heterogeneity in GACs, ctDNA-based NGS testing could provide more reliable results of MSI status, TMB, and genetic indicators for precision therapy (e.g., the fusion of *NTRK*) than tissue-based testing.

As for limitations, first, the DTIC result by IHC might not be as ample as the one calculated *in silico* from RNA-seq data. However, IHC provides histological illustration, enabling pathologists to score the DTIC in different regions. In the present study, we separately assess the DTICs in the central tumor area and invasive margin area. The correlations of NMP with invasive-margin DTICs were much weaker than its correlations with central-tumor DTICs, suggesting the potential distinction of the impacts of PI3K-AKT-mTOR on DTICs in tumor center and margin. Second, despite of this study with the largest sample size of GAC ICI-treatment cohort to date, the retrospective setting of our study may introduce biases, but this limitation has been minimized by the balanced characteristics in the NMP-high and NMP-low subgroups, and the implementation of subgroup analysis and multivariable analysis to exclude the confounding impacts from these variables. NMP held great promise by its broad applicability, for the high predictive value of ICI efficacy regardless of treatment lines, ECOG, pathology, NGS testing technique, TMB, and PD-L1 CPS making it a meaningful work for patient selection.

Conclusions

In conclusion, our findings demonstrate the heterogeneity of genotypes, DTICs, immune-related signatures, and immunotherapy efficacy in the dMMR/MSI-H GACs. Higher NMP, identified as a genomic correlate of lower DTICs in this population, might serve as a potential predictor of intrinsic resistance to anti-PD-(L)1 treatment. Additional studies are warranted to determine the synergistic effect of PI3K-AKT-mTOR inhibitors to overcome the resistance to ICI treatment in the NMP-high dMMR/MSI-H G/GEJ adenocarcinomas.

Abbreviations

dMMR: mismatch repair-deficient; MSI-H: microsatellite instability-high; GAC: gastric adenocarcinomas; DTICs: the density of tumor-infiltrating immune cells; ICI: immune checkpoint inhibitor; TCGA: the Cancer Genome Atlas cohort; NMP: the number of mutated genes in the PI3K-AKT-mTOR pathway; PD-L1: programmed death-ligand 1; PD-1: programmed death 1; CRC: colorectal cancer; G/GEJ: gastric or gastro-esophageal junction; TNM: tumor, node, and metastases; PCR: polymerase chain reaction; NGS: next-generation sequencing; HR: hazard ratio; DFS: disease-free survival; PFS: progression-free survival; OS: overall survival; ROC: receiver operating characteristic; CNV: copy number variation

Declarations

Ethics approval and consent to participate

Human samples and clinical data were collected and used in accordance with the principles of the Declaration of Helsinki and approved by the Ethics committee of Peking University Cancer Hospital. All

participants provided written informed consents. This report followed the Strengthening the Reporting of Observational Studies in Epidemiology (STROBE) reporting guideline.

Consent for publication

Not applicable.

Availability of data and materials

The datasets supporting the conclusions of this article are included within the article and its additional files.

Conflict of interest

Yu Xu, Bei Zhang, Chan Gao, Hui Chen, Xiaochen Zhao, and Jinping Cai are employees of the 3D Medicines Inc. Other authors declare no potential conflicts of interest.

Funding

This work was supported by the National Key Research and Development Program of China (No. 2017YFC1308900, to L. Shen), the Major Program of National Natural Science Foundation of China (No. 91959205, to L. Shen), and Special Scientific Research Key Project for Capital Health Development, China (No. 2018-2Z-1026, to Y. Sun).

Author contributions

Conception and design: Yu Xu, Yu Sun, and Lin Shen

Development of methodology: Zhenghang Wang, Xinyu Wang, Yu Xu, and Bei Zhang

Acquisition of data: Zhenghang Wang, Xinyu Wang, Yu Xu, Zhi Peng, Xiaotian Zhang, Jian Li, Yajie Hu, Xinya Zhao, Kun Dong, Bei Zhang, Hui Chen, and Xiaochen Zhao

Analysis and interpretation of data: Zhenghang Wang, Xinyu Wang, Yu Xu, Bei Zhang

Writing, review, and/or revision of the manuscript: Zhenghang Wang, Xinyu Wang, Yu Xu, Chan Gao, Xiaochen Zhao, Jinping Cai, Yuezong Bai, Yu Sun, and Lin Shen

Administrative, technical, or material support: Yuezong Bai, Yu Sun, and Lin Shen

Study supervision: Yu Sun, and Lin Shen

Final approval of manuscript: All authors

Acknowledgments

We thank Jingjie Bian (Brian) and Yao Jiang for their contributions to sample collection, all the included patients and their family members, and Dizai Shi (Stitch) for his emotional support.

References

1. Parsons MT, Buchanan DD, Thompson B, Young JP, Spurdle AB. Correlation of tumour BRAF mutations and MLH1 methylation with germline mismatch repair (MMR) gene mutation status: a literature review assessing utility of tumour features for MMR variant classification. J Med Genet. 2012;49(3):151-157. 10.1136/jmedgenet-2011-100714
2. Poynter JN, Siegmund KD, Weisenberger DJ, Long TI, Thibodeau SN, Lindor N, et al. Molecular characterization of MSI-H colorectal cancer by MLHI promoter methylation, immunohistochemistry, and mismatch repair germline mutation screening. Cancer Epidemiol Biomarkers Prev. 2008;17(11):3208-3215. 10.1158/1055-9965.Epi-08-0512
3. Latham A, Srinivasan P, Kemel Y, Shia J, Bandlamudi C, Mandelker D, et al. Microsatellite Instability Is Associated With the Presence of Lynch Syndrome Pan-Cancer. J Clin Oncol. 2019;37(4):286-295. 10.1200/jco.18.00283
4. Spies M, Fishel R. Mismatch repair during homologous and homeologous recombination. Cold Spring Harb Perspect Biol. 2015;7(3):a022657. 10.1101/cshperspect.a022657
5. Dudley JC, Lin MT, Le DT, Eshleman JR. Microsatellite Instability as a Biomarker for PD-1 Blockade. Clin Cancer Res. 2016;22(4):813-820. 10.1158/1078-0432.CCR-15-1678
6. Mandal R, Samstein RM, Lee KW, Havel JJ, Wang H, Krishna C, et al. Genetic diversity of tumors with mismatch repair deficiency influences anti-PD-1 immunotherapy response. Science. 2019;364(6439):485-491. 10.1126/science.aau0447
7. Lee V, Murphy A, Le DT, Diaz LA, Jr. Mismatch Repair Deficiency and Response to Immune Checkpoint Blockade. Oncologist. 2016;21(10):1200-1211. 10.1634/theoncologist.2016-0046
8. Angell HK, Lee J, Kim KM, Kim K, Kim ST, Park SH, et al. PD-L1 and immune infiltrates are differentially expressed in distinct subgroups of gastric cancer. Oncoimmunology. 2019;8(2):e1544442. 10.1080/2162402X.2018.1544442
9. Thompson ED, Zahurak M, Murphy A, Cornish T, Cuka N, Abdelfatah E, et al. Patterns of PD-L1 expression and CD8 T cell infiltration in gastric adenocarcinomas and associated immune stroma. Gut. 2017;66(5):794-801. 10.1136/gutjnl-2015-310839
10. Cho J, Chang YH, Heo YJ, Kim S, Kim NK, Park JO, et al. Four distinct immune microenvironment subtypes in gastric adenocarcinoma with special reference to microsatellite instability. ESMO Open. 2018;3(3):e000326. 10.1136/esmoopen-2018-000326
11. Le DT, Durham JN, Smith KN, Wang H, Bartlett BR, Aulakh LK, et al. Mismatch repair deficiency predicts response of solid tumors to PD-1 blockade. Science. 2017;357(6349):409-413. 10.1126/science.aan6733

12. Marabelle A, Le DT, Ascierto PA, Di Giacomo AM, De Jesus-Acosta A, Delord J-P, et al. Efficacy of Pembrolizumab in Patients With Noncolorectal High Microsatellite Instability/Mismatch Repair–Deficient Cancer: Results From the Phase II KEYNOTE-158 Study. J Clin Oncol. 2019;38(1):1-10. 10.1200/JCO.19.02105
13. Sveen A, Johannessen B, Tengs T, Danielsen SA, Eilertsen IA, Lind GE, et al. Multilevel genomics of colorectal cancers with microsatellite instability-clinical impact of JAK1 mutations and consensus molecular subtype 1. Genome Med. 2017;9(1):46. 10.1186/s13073-017-0434-0
14. Yang Y, Shi Z, Bai R, Hu W. Heterogeneity of MSI-H gastric cancer identifies a subtype with worse survival. J Med Genet. 2020. 10.1136/jmedgenet-2019-106609
15. Bray F, Ferlay J, Soerjomataram I, Siegel RL, Torre LA, Jemal A. Global cancer statistics 2018: GLOBOCAN estimates of incidence and mortality worldwide for 36 cancers in 185 countries. CA Cancer J Clin. 2018. 10.3322/caac.21492
16. Cortes-Ciriano I, Lee S, Park WY, Kim TM, Park PJ. A molecular portrait of microsatellite instability across multiple cancers. Nat Commun. 2017;8(15180. 10.1038/ncomms15180
17. Hause RJ, Pritchard CC, Shendure J, Salipante SJ. Classification and characterization of microsatellite instability across 18 cancer types. Nature medicine. 2016;22(11):1342-1350. 10.1038/nm.4191
18. Fu T, Gong F, Xu Y. 83MO Co-occurrence of actionable gene fusions and microsatellite instability-high (MSI-H) in 20296 solid tumors: A pan-cancer analysis. Ann Oncol. 2020;31(S274. 10.1016/j.annonc.2020.08.204
19. Tamborero D, Rubio-Perez C, Muinos F, Sabarinathan R, Piulats JM, Muntasell A, et al. A Pan-cancer Landscape of Interactions between Solid Tumors and Infiltrating Immune Cell Populations. Clin Cancer Res. 2018;24(15):3717-3728. 10.1158/1078-0432.CCR-17-3509
20. Cancer Genome Atlas Research N. Comprehensive molecular characterization of gastric adenocarcinoma. Nature. 2014;513(7517):202-209. 10.1038/nature13480
21. Adzhubei IA, Schmidt S, Peshkin L, Ramensky VE, Gerasimova A, Bork P, et al. A method and server for predicting damaging missense mutations. Nat Methods. 2010;7(4):248-249. 10.1038/nmeth0410-248
22. Ng PC, Henikoff S. Predicting deleterious amino acid substitutions. Genome Res. 2001;11(5):863-874. 10.1101/gr.176601
23. Yu Y, Ma X, Zhang Y, Zhang Y, Ying J, Zhang W, et al. Changes in Expression of Multiple Checkpoint Molecules and Infiltration of Tumor Immune Cells after Neoadjuvant Chemotherapy in Gastric Cancer. J Cancer. 2019;10(12):2754-2763. 10.7150/jca.31755
24. Chen HY, Xu L, Li LF, Liu XX, Gao JX, Bai YR. Inhibiting the CD8(+) T cell infiltration in the tumor microenvironment after radiotherapy is an important mechanism of radioresistance. Sci Rep. 2018;8(1):11934. 10.1038/s41598-018-30417-6
25. Tada Y, Togashi Y, Kotani D, Kuwata T, Sato E, Kawazoe A, et al. Targeting VEGFR2 with Ramucirumab strongly impacts effector/ activated regulatory T cells and CD8(+) T cells in the tumor

microenvironment. J Immunother Cancer. 2018;6(1):106. 10.1186/s40425-018-0403-1

26. Hu W, Yang Y, Qi L, Chen J, Ge W, Zheng S. Subtyping of microsatellite instability-high colorectal cancer. Cell Commun Signal. 2019;17(1):79. 10.1186/s12964-019-0397-4
27. Shitara K, Özgüroğlu M, Bang Y-J, Di Bartolomeo M, Mandalà M, Ryu M-h, et al. The association of tissue tumor mutational burden (tTMB) using the Foundation Medicine genomic platform with efficacy of pembrolizumab versus paclitaxel in patients (pts) with gastric cancer (GC) from KEYNOTE-061. J Clin Oncol. 2020;38(15_suppl):4537-4537. 10.1200/JCO.2020.38.15_suppl.4537
28. Fuchs CS, Özgüroğlu M, Bang Y-J, Di Bartolomeo M, Mandalà M, Ryu M-h, et al. The association of molecular biomarkers with efficacy of pembrolizumab versus paclitaxel in patients with gastric cancer (GC) from KEYNOTE-061. J Clin Oncol. 2020;38(15_suppl):4512-4512. 10.1200/JCO.2020.38.15_suppl.4512
29. Fukuoka S, Hara H, Takahashi N, Kojima T, Kawazoe A, Asayama M, et al. Regorafenib Plus Nivolumab in Patients With Advanced Gastric or Colorectal Cancer: An Open-Label, Dose-Escalation, and Dose-Expansion Phase Ib Trial (REGONIVO, EPOC1603). J Clin Oncol. 2020:JCO.19.03296. 10.1200/JCO.19.03296
30. Herbst RS, Arkenau HT, Santana-Davila R, Calvo E, Paz-Ares L, Cassier PA, et al. Ramucirumab plus pembrolizumab in patients with previously treated advanced non-small-cell lung cancer, gastro-oesophageal cancer, or urothelial carcinomas (JVDF): a multicohort, non-randomised, open-label, phase 1a/b trial. Lancet Oncol. 2019. 10.1016/S1470-2045(19)30458-9
31. Shitara K, Ozguroglu M, Bang YJ, Di Bartolomeo M, Mandala M, Ryu MH, et al. Pembrolizumab versus paclitaxel for previously treated, advanced gastric or gastro-oesophageal junction cancer (KEYNOTE-061): a randomised, open-label, controlled, phase 3 trial. Lancet. 2018;392(10142):123-133. 10.1016/S0140-6736(18)31257-1
32. Fuchs CS, Doi T, Jang RW, Muro K, Satoh T, Machado M, et al. Safety and Efficacy of Pembrolizumab Monotherapy in Patients With Previously Treated Advanced Gastric and Gastroesophageal Junction Cancer: Phase 2 Clinical KEYNOTE-059 Trial. JAMA Oncol. 2018;4(5):e180013. 10.1001/jamaoncol.2018.0013
33. Kang YK, Boku N, Satoh T, Ryu MH, Chao Y, Kato K, et al. Nivolumab in patients with advanced gastric or gastro-oesophageal junction cancer refractory to, or intolerant of, at least two previous chemotherapy regimens (ONO-4538-12, ATTRACTION-2): a randomised, double-blind, placebo-controlled, phase 3 trial. Lancet. 2017;390(10111):2461-2471. 10.1016/S0140-6736(17)31827-5
34. Wang F, Wei XL, Wang FH, Xu N, Shen L, Dai GH, et al. Safety, efficacy and tumor mutational burden as a biomarker of overall survival benefit in chemo-refractory gastric cancer treated with toripalimab, a PD1 antibody in phase Ib/II clinical trial NCT02915432. Ann Oncol. 2019. 10.1093/annonc/mdz197
35. Chida K, Kawazoe A, Kawazu M, Suzuki T, Nakamura Y, Nakatsura T, et al. A Low Tumor Mutational Burden and PTEN Mutations Are Predictors of a Negative Response to PD-1 Blockade in MSI-

H/dMMR Gastrointestinal Tumors. Clin Cancer Res. 2021;27(13):3714-3724. 10.1158/1078-0432.CCR-21-0401

36. Kwon M, An M, Klempner SJ, Lee H, Kim KM, Sa JK, et al. Determinants of Response and Intrinsic Resistance to PD-1 Blockade in Microsatellite Instability-High Gastric Cancer. Cancer Discov. 2021. 10.1158/2159-8290.CD-21-0219
37. Zhang K, Hong X, Song Z, Xu Y, Li C, Wang G, et al. Identification of deleterious NOTCH mutation as novel predictor to efficacious immunotherapy in NSCLC. Clin Cancer Res. 2020. 10.1158/1078-0432.CCR-19-3976
38. Loupakis F, Depetris I, Biason P, Intini R, Prete AA, Leone F, et al. Prediction of Benefit from Checkpoint Inhibitors in Mismatch Repair Deficient Metastatic Colorectal Cancer: Role of Tumor Infiltrating Lymphocytes. Oncologist. 2020. 10.1634/theoncologist.2019-0611
39. Schrock AB, Ouyang C, Sandhu J, Sokol E, Jin D, Ross JS, et al. Tumor mutational burden is predictive of response to immune checkpoint inhibitors in MSI-high metastatic colorectal cancer. Ann Oncol. 2019. 10.1093/annonc/mdz134
40. Siddiqui I, Schaeuble K, Chennupati V, Fuertes Marraco SA, Calderon-Copete S, Pais Ferreira D, et al. Intratumoral Tcf1(+)PD-1(+)CD8(+) T Cells with Stem-like Properties Promote Tumor Control in Response to Vaccination and Checkpoint Blockade Immunotherapy. Immunity. 2019;50(1):195-211 e110. 10.1016/j.immuni.2018.12.021
41. Rooney MS, Shukla SA, Wu CJ, Getz G, Hacohen N. Molecular and genetic properties of tumors associated with local immune cytolytic activity. Cell. 2015;160(1-2):48-61. 10.1016/j.cell.2014.12.033
42. Liu Y, Sethi NS, Hinoue T, Schneider BG, Cherniack AD, Sanchez-Vega F, et al. Comparative Molecular Analysis of Gastrointestinal Adenocarcinomas. Cancer Cell. 2018;33(4):721-735 e728. 10.1016/j.ccell.2018.03.010
43. Okkenhaug K, Graupera M, Vanhaesebroeck B. Targeting PI3K in Cancer: Impact on Tumor Cells, Their Protective Stroma, Angiogenesis, and Immunotherapy. Cancer Discov. 2016;6(10):1090-1105. 10.1158/2159-8290.CD-16-0716
44. Marijt KA, Sluijter M, Blijleven L, Tolmeijer SH, Scheeren FA, van der Burg SH, et al. Metabolic stress in cancer cells induces immune escape through a PI3K-dependent blockade of IFNgamma receptor signaling. J Immunother Cancer. 2019;7(1):152. 10.1186/s40425-019-0627-8
45. Sai J, Owens P, Novitskiy SV, Hawkins OE, Vilgelm AE, Yang J, et al. PI3K Inhibition Reduces Mammary Tumor Growth and Facilitates Antitumor Immunity and Anti-PD1 Responses. Clin Cancer Res. 2017;23(13):3371-3384. 10.1158/1078-0432.CCR-16-2142
46. Borcoman E, De La Rochere P, Richer W, Vacher S, Chemlali W, Krucker C, et al. Inhibition of PI3K pathway increases immune infiltrate in muscle-invasive bladder cancer. Oncoimmunology. 2019;8(5):e1581556. 10.1080/2162402X.2019.1581556
47. Atefi M, Avramis E, Lassen A, Wong DJ, Robert L, Foulad D, et al. Effects of MAPK and PI3K pathways on PD-L1 expression in melanoma. Clin Cancer Res. 2014;20(13):3446-3457.

10.1158/1078-0432.CCR-13-2797

Tables

Table 1. Response to immunotherapy in the ICI treatment cohort.

	Total (n=36)	NMP=0/1 (n=16)	NMP≥2 (n=20)	P value
CR	5 (13.9%)	5 (31.3%)	0 (0.0%)	
PR	12 (33.3%)	7 (43.8%)	5 (25.0%)	
Non-CR/non-PD	5 (13.9%)	2 (12.5%)	3 (15.0%)	
Stable disease	3 (8.3%)	1 (6.3%)	2 (10.0%)	
PD	9 (25.0%)	1 (6.3%)	8 (40.0%)	
No assessment*	2 (5.6%)	0 (0%)	2 (10.0%)	
ORR in modified population (n=31)**	54.8%	85.7%	29.4%	0.002
4-month PFS rate (n=32)***	62.5%	93.3%	35.3%	0.001

Abbreviations: CR=complete response, ORR=objective response rate, PD=progressive disease, PFS=progressive-free disease, PR=partial response.

*No assessment represents the patients who had a baseline assessment but no post-baseline assessment at the time of the data cutoff date, due to death before the first post-baseline radiologic imaging assessment.

**Modified population represents the patients with evaluable target lesion.

***Four patients who have been followed up for less than four months and have not yet progressed were excluded from the analysis of 4-month PFS rate.

Figures

Figure 1

Clinicopathological and genomic characteristics of the surgery cohort. A. Illustration of clinicopathological and genomic characteristics of the surgery cohort. Tumor mutational burden is shown in the upper panel. Basic clinicopathological characteristics are illustrated in the middle panel. Mutations with high frequencies are depicted in the lower panel. B. Enriched genes mutated in concordant dMMR/MSI-H samples (highlighted in pink) or pMMR/MSS samples (highlighted in blue). C. TMB, CNV,

and fusion in concordant dMMR/MSI-H samples, discordant samples, and concordant pMMR/MSS samples. D. Heatmap of the number of mutations in pre-specified pathways in concordant samples. Abbreviations: dMMR=mismatch repair-deficient, EBV=Epstein-Barr virus, FISH=fluorescence in situ hybridization, HER2=human epidermal growth factor receptor 2, IHC=immunohistochemistry, MLH1=MutL homolog 1, MMR=mismatch repair, MSH2=MutS Homolog 2, MSH6=MutS Homolog 6, MSI-H=microsatellite instability-high, MSI-L=microsatellite instability-low, MSS=microsatellite stability, N.A.=not applicable, NGS=next-generation sequencing, PCR=polymerase chain reaction, PMS2=PMS1 Homolog 2, TMB=tumor mutational burden, CNV=copy number variation .

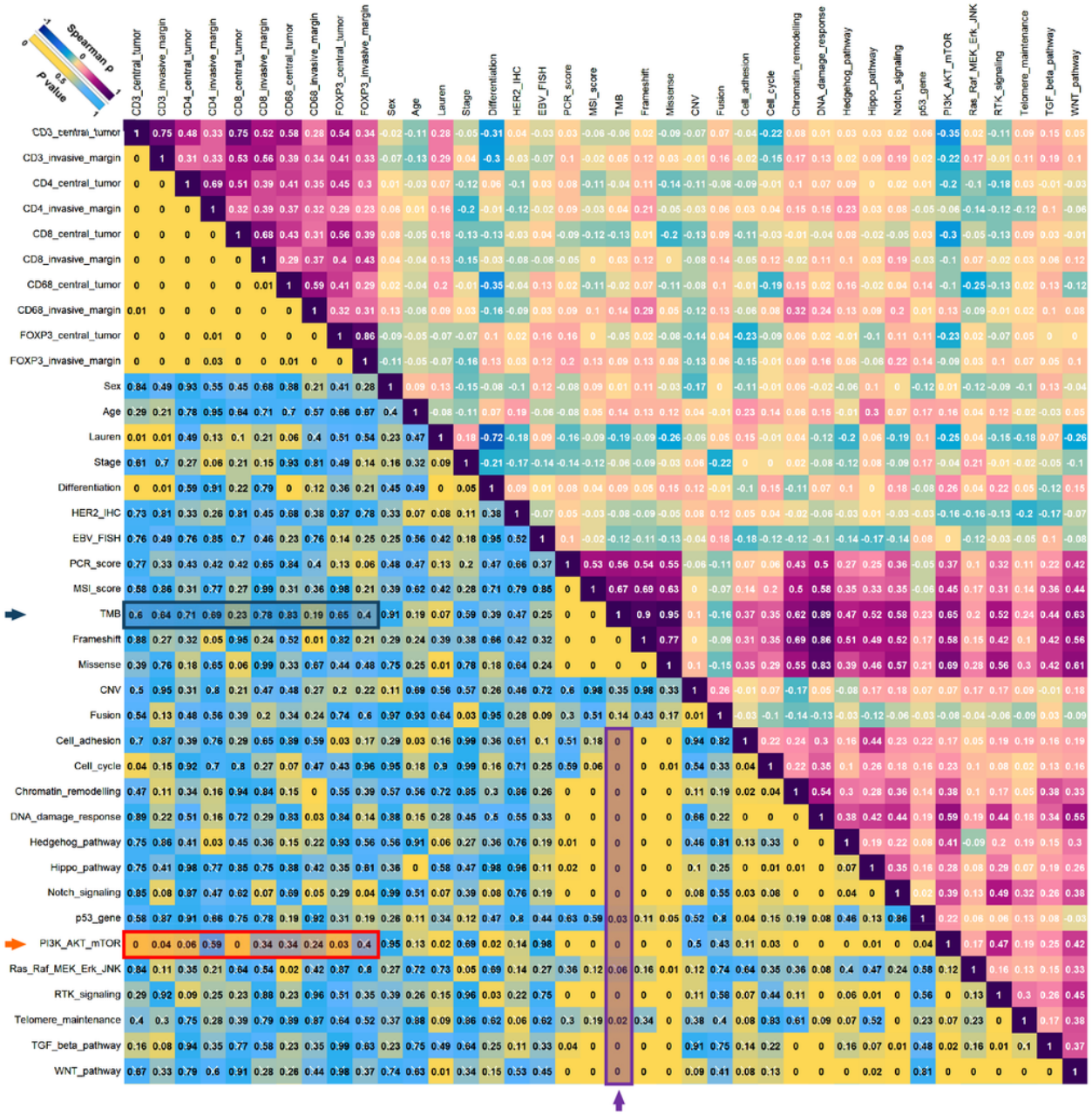

Figure 2

Correlates of immune cell infiltration in dMMR/MSI-H gastric adenocarcinomas without receiving neoadjuvant chemotherapy. Correlation matrix of NAC-naïve concordant dMMR/MSI-H samples in the surgery cohort. The values in the upper right part refer to the Spearman ρ, and the values in the lower left part indicate p values. The scales of colors are shown at the upper left corner. Abbreviations: CNV=copy number variation, dMMR=mismatch repair-deficient, EBV=Epstein-Barr virus, FISH=fluorescence in situ hybridization, HER2=human epidermal growth factor receptor 2, IHC=immunohistochemistry, MLH1=MutL homolog 1, MMR=mismatch repair, MSH2=MutS Homolog 2, MSH6=MutS Homolog 6, MSI=microsatellite instability, MSI-H=microsatellite instability-high, MSI-L=microsatellite instability-low, MSS=microsatellite stability, N.A.=not applicable, NAC=neoadjuvant chemotherapy, NGS=next-generation sequencing, PCR=polymerase chain reaction, PMS2=PMS1 Homolog 2, RTK=receptor tyrosine kinase, TGF=transforming growth factor, TMB=tumor mutational burden.

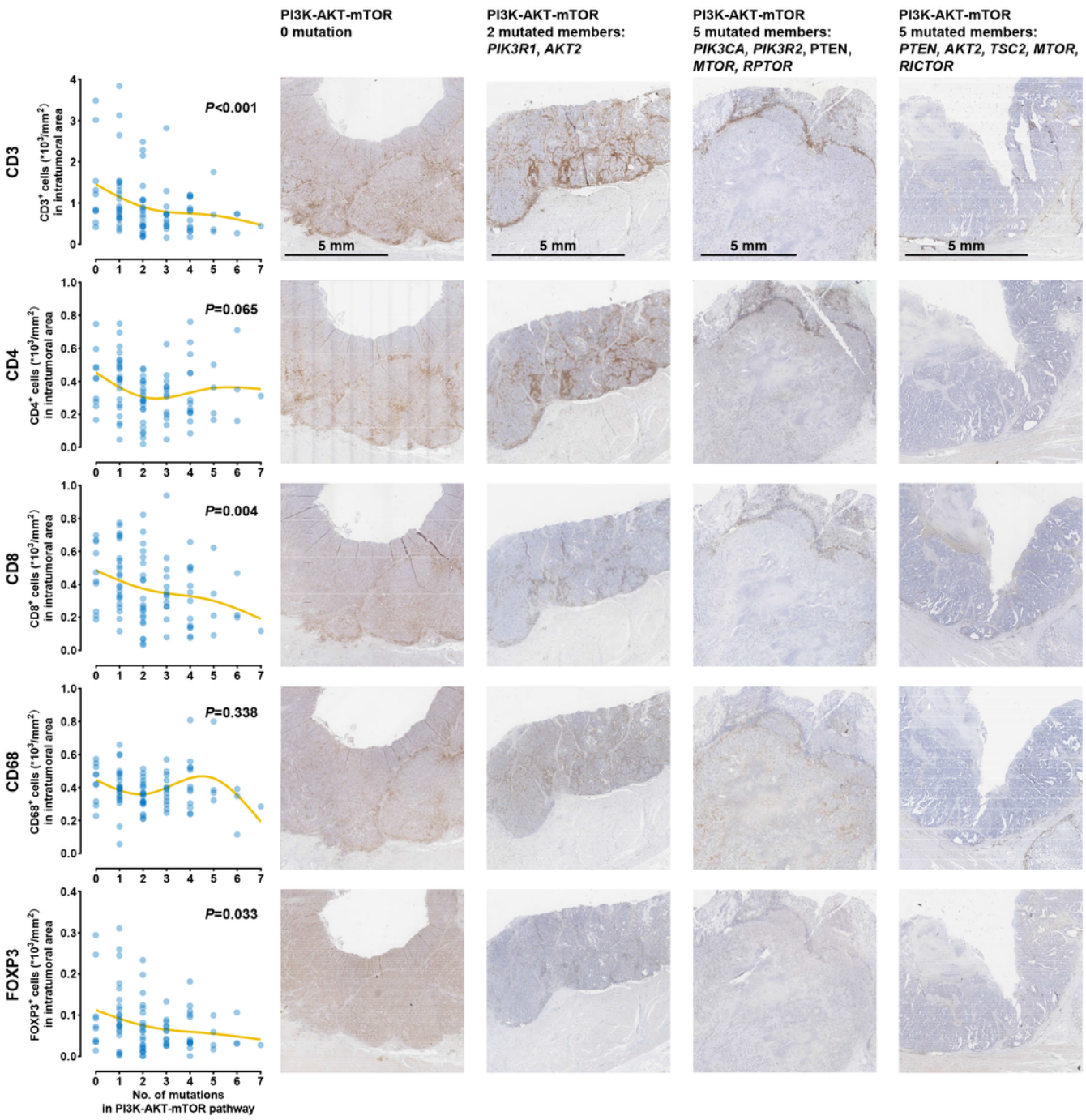

Figure 3

Association between NMP and immune cell infiltration in dMMR/MSI-H gastric adenocarcinomas without receiving neoadjuvant chemotherapy. Correlation of NMP with DITCs, including CD3+, CD4+, CD8+, and FOXP3+ cells in central tumor area (left part). Immunohistochemical staining of the representative samples for CD3, CD4, CD8, CD68, and FOXP3 (right part). Scale bar: 5 mm. Every blue point indicates the data of one sample, and the yellow lines are smoothing splines illustrating the trend of association between NMP and DITCs. Abbreviations: DTIC=density of tumor-infiltrating immune cell,

dMMR=mismatch repair-deficient, MSI-H=microsatellite instability-high, NMP=number of mutated members of the PI3K-AKT-mTOR pathway.

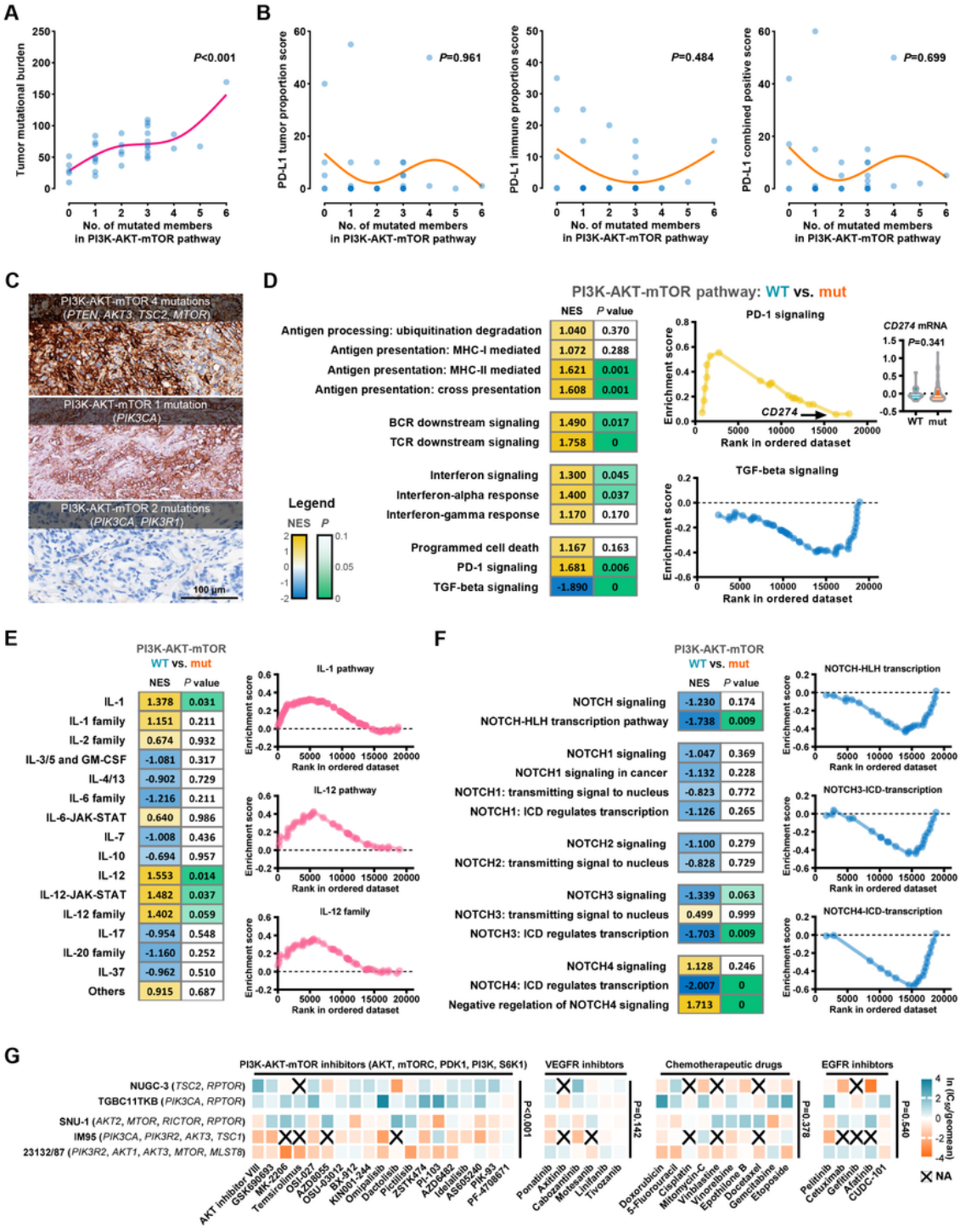

Figure 4

Immune correlates of genetic aberration in PI3K-AKT-mTOR pathway. A. Correlation between NMP and TMB. Every blue point indicates the data of one sample, and the pink line is a smoothing spline illustrating the trend of association between NMP and TMB. B. Correlation between NMP and PD-L1

expression (TPS, IPS, and CPS). Every blue point indicates the data of one sample, and the orange line is a smoothing spline illustrating the trend of association between NMP and PD-L1 expression. C. Representative images of PD-L1 staining. D. GSEA of gene signatures related to immune activation in comparisons between samples with or without mutation in PI3K-AKT-mTOR pathway. The yellow-blue scale represents NES. The green scale represents P value. The plots of enrichment scores of PD-1 signaling, and TGF-β signaling, together with the comparisons of PD-L1 (CD274) mRNA expression. E-F. GSEA of gene signatures related to interleukin pathways (E), and NOTCH signaling (F) in comparisons between samples with or without mutation in PI3K-AKT-mTOR pathway. The yellow-blue scale represents NES. The green scale represents P value. G. Drug sensitivity of the five MSI-H STAD cell lines.
Abbreviations: BCR=B cell receptor, CPS=combined positive score, IL=interleukin, IPS=immune proportion score, MHC=major histocompatibility complex, NES=normalized enrichment score, NMP=number of mutated members in the PI3K-AKT-mTOR pathway, PD-1=programmed death-1, PD-L1=programmed death-ligand 1, TCR=T cell receptor, TGF=transforming growth factor, TMB=tumor mutational burden, TPS=tumor proportion score, WT=wildtype.

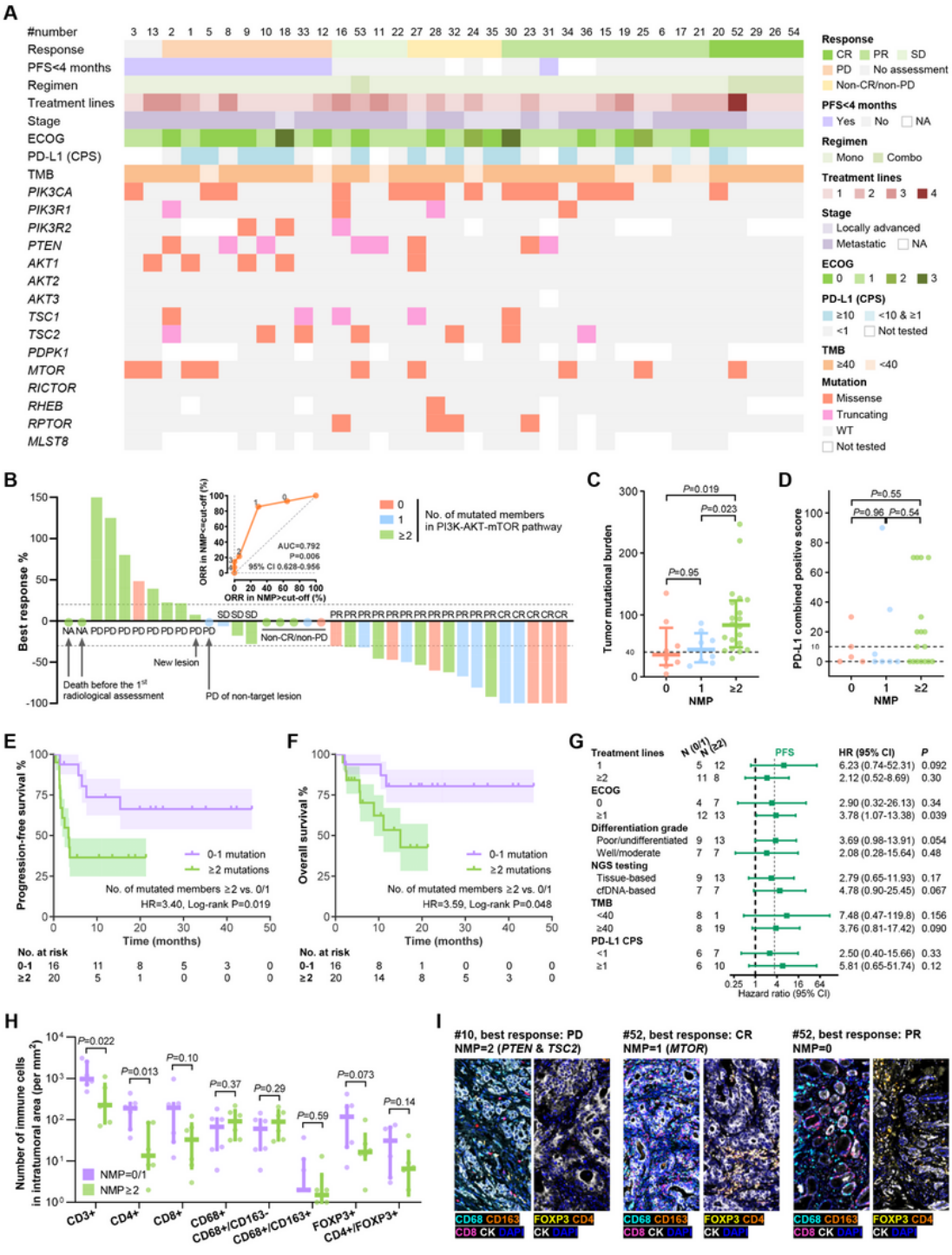

Figure 5

Association between NMP and response to ICI in dMMR/MSI-H G/GEJ adenocarcinomas. A. Basic clinicopathological characteristics and mutations of the PI3K-AKT-mTOR pathway of the ICI treatment cohort. B. Bar plot illustrating best response and ROC curve of the NMP to predict ORR. The NMP of each patient is labeled with red (NMP=0), blue (NMP=1), and green (NMP>1). C-D. Association of NMP with tumor mutational burden (C) and PD-L1 CPS score (D). E-F. Kaplan-Meier curves of PFS (E) and OS (F) in

the NMP-low (0/1) and NMP-high (>1) patients. G. Subgroup analysis of PFS. H. Association between NMP and DTICs. I. Representative images of DTICs. Abbreviations: AUC=area under curve, CI=confidence interval, CPS=combined positive score, CR=complete response, DTIC=density of tumor-infiltrating immune cells, ECOG=Eastern Cooperative Oncology Group, HR=hazard ratio, NA=not applicable, ORR=objective response rate, OS=overall survival, PD=progressive disease, PD-L1=programmed death-ligand 1, PFS=progression-free survival, PR=partial response, SD=stable disease, WT=wildtype.

Supplementary Files

This is a list of supplementary files associated with this preprint. Click to download.

- Onlineonlysupplement.docx